

Partially stochastic deep learning with uncertainty quantification for model predictive heating control

Emma Hannula^{a,c,*}, Arttu Häkkinen^{a,b,*}, Felipe Uribe^{a,b}, Antti Solonen^{a,b}, Jana de Wiljes^{a,c}, Lassi Roininen^a

^a*LUT University, Yliopistonkatu 34, Lappeenranta, 53850, Finland*

^b*Danfoss Leanheat, Ilmalantori 1, Helsinki, 00240, Finland*

^c*TU Ilmenau, Ehrenbergstraße 29, Ilmenau, 98693, Germany*

Abstract

Improving the energy efficiency of building heating systems is crucial for reducing global energy consumption and greenhouse gas emissions. Traditional control methods rely on static heating curves that are based solely on outdoor temperature, neglecting system state measurements, such as indoor temperature, and free heat sources, such as solar gain. A more effective strategy is model predictive control (MPC), which optimizes heating control by incorporating system state predictions based on weather forecasts, among other factors. However, current industrial MPC solutions often employ simplified physics-inspired indoor temperature models, sacrificing accuracy for robustness and interpretability. While purely data-driven models offer superior predictive performance, they face challenges such as overfitting and lack of transparency.

To bridge this gap, we propose a partially stochastic deep learning (DL) architecture for building-specific indoor temperature modeling. Unlike most studies that evaluate model performance through simulations or limited test buildings, our experiments across a large dataset of 100 real-world buildings, covering various heating season conditions, demonstrate that the proposed model outperforms a widely used industrial physics-based model in predictive accuracy. The median prediction error over 100,000 test samples was reduced by 25% for a 1-hour prediction horizon, 34% for a 6-hour horizon, and 41% for a 48-hour horizon—the longest horizon for which weather forecasts are reasonably accurate. Thus, the proposed DL architecture shows significant potential to improve thermal comfort and energy efficiency in heating MPC solutions. Although its computational cost is higher than that of the reference model, we discuss why this trade-off is manageable, even in large-scale applications. Unlike deterministic black-box approaches, the partially stochastic DL model offers a critical advantage by enabling pre-assessment of model feasibility through predictive uncertainty quantification. This work advances heating MPC, particularly for buildings with comprehensive datasets on their thermal behavior under various weather conditions.

Keywords: model predictive control, variational inference, long short-term memory, Bayesian neural networks, uncertainty quantification, central heating systems

1. Introduction and scope

The heating of buildings contributes significantly to global energy consumption and greenhouse gas emissions [1, 2, 3, 4], especially in northern climates characterized by long and cold winters [5]. Global warming and Europe’s recent energy crisis further underscore the need for energy-efficient heating solutions.

Water-based central heating systems, often utilizing district heating as the heat source, are prevalent in northern climates, particularly in urban multi-apartment buildings. These systems consist of two networks separated by heat exchangers: the primary side (connected to the heat source) and the secondary side (distributing heat within the building). The secondary side typically includes circuits for domestic hot water and space heating. A heat controller adjusts the primary side flow via control valves to regulate secondary side temperatures. This study focuses on Nordic residential buildings equipped with radiator or underfloor heating systems.

*Corresponding authors. These authors contributed equally to this work.

Email addresses: emma.hannula@lut.fi (Emma Hannula), arttu.hakkinen@lut.fi (Arttu Häkkinen)

Traditional control methods rely on a deterministic heating curve, adjusting the space heating supply temperature reactively based on measured outdoor temperature. However, this open-loop approach lacks feedback on the system’s state (indoor temperature), often leading to inefficiencies through overheating or underheating. It also lacks the ability to anticipate sudden weather changes and account for factors that introduce free heat into the system, such as solar irradiation and internal heat sources (e.g., occupants and electronic devices). The thermal dynamics of buildings are constantly evolving, making the determination of a suitable heating curve a process of endless trial and error, or requiring expensive expert services or complex physics-based white-box modeling.

These shortcomings can be addressed with model predictive control (MPC), which closes the feedback loop by utilizing system state measurements and weather forecasts to plan control actions for the future [6, 7]. Predictive indoor temperature models formulated to capture thermal dynamics of the building are central to MPC, allowing the inclusion of factors such as solar irradiation and temporal disturbances from internal heat sources. These models adapt to the existing heating dynamics of buildings through automatic updates based on new data. Consequently, MPC provides actual control of the state of the system, often resulting in reduced energy consumption.

The primary objectives of building heating—thermal comfort and energy efficiency—are generally achieved by maintaining the system state at a predefined target. However, MPC enables the incorporation of more advanced heating optimization objectives. For instance, peak load minimization can be achieved by shifting the heating load based on weather forecasts, predictive modeling, and temporal profiles of domestic hot water usage derived from consumption data. In addition, district heating utilities can leverage large stocks of MPC-controlled buildings as a demand response tool, using them as thermal storage in conjunction with their production optimization. This is feasible because heat loads within buildings can be controlled with greater precision. To realize these benefits, accurate indoor temperature predictions are essential, particularly for longer prediction horizons.

MPC applications can be classified based on the approach to indoor temperature modeling: white-box, gray-box, and black-box models [8]. White-box models are fully physics-based, relying on theoretical principles of heat transfer, energy conservation, and building metadata. Although they offer complete transparency, they are often impractical for scalable solutions. Gray-box models integrate physics-inspired equations with statistical parameter estimation. These models are robust and interpretable, but tend to oversimplify complex dynamics, such as thermal lag effects. Black-box models are purely data-driven alternatives, capable of capturing complex nonlinear relationships when large, descriptive datasets on system inputs and state evolution are available. However, they risk overfitting and lack transparency, necessitating comprehensive datasets and methods to pre-evaluate prediction feasibility to be viable for real-world applications [9].

In industrial heating MPC solutions, the choice of indoor temperature modeling approach can vary based on the comprehensiveness of the available building-specific dataset and regular evaluations of the models’ predictive performance and uncertainty. These evaluations can consider, for instance, how accurately the models capture each building’s thermal behavior based on recent data and how uncertain the models are about their predictions given the forecasted weather conditions. Thus, the model with the best potential can be selected for each building and prediction scenario.

In this work, we aim to develop an accurate probabilistic indoor temperature model that allows for pre-assessment of model feasibility through predictive uncertainty quantification. This model can be used in heating MPC for buildings with comprehensive historical datasets across various weather conditions, provided the uncertainty in its predictions is sufficiently low.

1.1. Related work

Research in machine learning for time series modeling has primarily focused on exploring Recurrent Neural Networks (RNNs) for specific applications. For instance, Ramadan et al. [10] applied multiple machine learning methods for indoor temperature prediction and compared their performance against a resistance-capacity gray-box model. Among these techniques, Long Short-Term Memory (LSTM), a type of RNN, has demonstrated superior accuracy [11, 12, 13]. Recent studies have aimed to enhance LSTM accuracy by employing methods such as feature extraction with convolutional layers [14] and incorporating an encoder-decoder architecture with Bayesian hyperparameter optimization [15]. Fang et al. [16] highlighted the effectiveness of LSTM models when trained on extensive datasets, such as three years of data. Despite promising results, many of these methods are primarily validated through simulations and lack application to real-world buildings [17].

Existing applications of uncertainty quantification in machine learning for time series models encompass several approaches. The Bayesian RNN model discussed in [18], which employs a sequential approach to

update network parameters and hyperparameters, outperforms several traditional time series modeling methods. Another development is the quantile RNN model proposed in [19], which directly learns prediction intervals as lower and upper bounds; this model effectively handles multiple time series, shifting seasonality, future planned event spikes, and cold-starts in large-scale forecasting scenarios. Frequentist approaches to uncertainty estimation are also available. For instance, the method in [20] derives predictive uncertainty from the variability of the RNN output’s sampling distribution; this is achieved by repeatedly removing sections of temporally correlated training data and collecting predictions from the RNN re-trained on the remaining data. Conformal prediction has gained popularity as a frequentist method for constructing distribution-free prediction intervals. However, since this approach requires data exchangeability, which is often not applicable in time series, the methods in [21, 22] propose techniques to extend its applicability to time series data.

1.2. Contributions and novelty

- (i) For our comparative experiments, we derive and introduce a Bayesian gray-box model for building-specific indoor temperature modeling as the reference method. This reference model has been successfully integrated into a real-world MPC solution, currently operating across thousands of centrally-heated buildings in Northern Europe. Thus, it serves as a relevant baseline model for comparative studies aimed at developing more accurate indoor temperature models for large-scale industrial MPC solutions.
- (ii) We propose a partially stochastic deep learning architecture for building-specific indoor temperature modeling. Compared to deterministic black-box methods, the proposed model allows pre-assessment of its feasibility through predictive uncertainty quantification, with minimal sacrifice in predictive performance. Although the computational cost of the proposed model is higher than that of the reference model, we discuss why this poses no issue for large-scale applications due to the implementation strategies in real-world MPC solutions.
- (iii) Our experiments, conducted on a comprehensive real-world dataset from 100 buildings under various weather conditions, demonstrate that the partially stochastic deep learning model achieves superior predictive performance compared to the reference model for both short- and long-term prediction horizons. Therefore, implementing the proposed model in a heating MPC solution for buildings with sufficiently descriptive datasets on their thermal behavior, and when the predictive uncertainty is sufficiently low, would improve the control of centrally-heated buildings due to more accurate indoor temperature modeling. This would enhance heating control in terms of indoor comfort, energy efficiency, peak load minimization, and advanced demand response solutions.

We emphasize that the aim of this study is not to develop a physics-based indoor temperature model, but to create an accurate probabilistic model that captures complex thermodynamic relationships within the system based on high-quality data from diverse conditions. This model also enables the assessment of its suitability under various prediction circumstances by quantifying the uncertainty in its predictions.

1.3. Structure of the paper

The rest of the paper is organized as follows. In Section 2, we introduce the reference model and the DL models. Section 3 covers the dataset, the experiments and their implementation, and the results. Section 4 presents the concluding remarks of the study.

2. Methodology

We introduce the reference gray-box model and the deep learning models for predicting the indoor temperature of a centrally-heated residential building. Both the reference model and the partially stochastic DL model incorporate built-in uncertainty quantification. Therefore, we begin by discussing the theoretical principles of the Bayesian framework.

2.1. Bayesian inference

In the Bayesian framework, model unknowns are represented by probability distributions, inherently incorporating existing uncertainty [23]. Bayesian inference allows for updating beliefs about unknown quantities \mathbf{Z} in a mathematical model given observed data $\mathbf{y} \sim \mathbf{Y}$. Bayesian inference is fundamentally based on Bayes’ theorem, with its main components being the *prior*, the *likelihood*, and the *posterior*.

- The prior distribution $p(\mathbf{Z})$ expresses initial beliefs, assumptions, or knowledge about \mathbf{Z} without observing any data.
- The likelihood function $p(\mathbf{y} | \mathbf{Z})$ quantifies the probability of observing the data \mathbf{y} given a specific realization of the unknown quantity $\mathbf{Z} = \mathbf{z}$, reflecting how well the observations support the computational model.
- The posterior distribution $p(\mathbf{Z} | \mathbf{y})$ represents the updated beliefs about \mathbf{Z} after observing \mathbf{y} . It combines the prior assumptions with the new information provided by the data through Bayes' theorem:

$$p(\mathbf{Z} | \mathbf{y}) = \frac{p(\mathbf{y} | \mathbf{Z})p(\mathbf{Z})}{p(\mathbf{y})}, \quad (1)$$

where $p(\mathbf{y}) = \int p(\mathbf{y} | \mathbf{Z}) d\mathbf{p}(\mathbf{Z})$ is the *marginal likelihood* or *evidence*, acting as a normalizing constant.

The primary objective of Bayesian inference is to find the posterior probability density $p(\mathbf{Z} | \mathbf{y})$. In practice, this task is often computationally intractable, primarily due to the high dimensionality of \mathbf{Z} and the complexity of the computational model. As a result, approximations are often necessary.

2.1.1. Variational inference

The posterior can be approximated using sampling-based methods such as Markov Chain Monte Carlo (MCMC) [23], or via the framework of *variational inference* [24, 25, 26, 27]. While MCMC often achieves more precise approximations, variational inference is significantly more computationally efficient. Hence, for the posterior inference of the models covered in this study for large-scale industrial solutions, we focus on variational inference.

In variational inference, the goal is to identify the reference parameters of a tractable variational distribution $q(\mathbf{Z})$ such that it approximates the true posterior $p(\mathbf{Z} | \mathbf{y})$ as closely as possible [26]. This closeness is measured using the Kullback–Leibler (KL) divergence, which measures the dissimilarity between two distributions:

$$D_{\text{KL}}(q(\mathbf{Z}) \parallel p(\mathbf{Z} | \mathbf{y})) = \int q(\mathbf{Z}) \log \left(\frac{q(\mathbf{Z})}{p(\mathbf{Z} | \mathbf{y})} \right) d\mathbf{Z} \geq 0. \quad (2)$$

Consequently, the problem of posterior inference is transformed into an optimization problem of minimizing the KL divergence in (2), equivalent to maximizing the evidence lower bound (ELBO) [24, 25]

$$\text{ELBO}(q) = \mathbb{E}_q [\log p(\mathbf{y} | \mathbf{Z})] - D_{\text{KL}}(q(\mathbf{Z}) \parallel p(\mathbf{Z})), \quad (3)$$

to achieve the tightest bound on the logarithmic marginal likelihood $\log p(\mathbf{y})$

Maximizing (3) with respect to $q(\mathbf{Z})$ can be achieved using various methods, typically ensuring tractability by assuming the unknowns are independent and factorizing according to the mean-field approximation [25] as:

$$q(\mathbf{Z}) = \prod_i q(\mathbf{Z}_i). \quad (4)$$

Although there are specific forms of variational families for which the optimization problem can be solved in closed form, in practice, this is typically feasible only for distributions from the conjugate exponential family.

2.2. Reference model

Under steady-state conditions, we consider the air mass inside a building as a system, separated from its surroundings by the building envelope (see Figure 1). The system, the envelope, and surroundings are treated separately as homogeneous media with their own uniform thermal properties. Although buildings typically have multiple thermal zones, we simplify the inner volume to a single room. Furthermore, we assume the envelope has minimal thermal capacitance, acting solely as a thermal resistor for heat flow between the system and the environment.

This first-order nodal view of a highly complex and time-varying dynamical system [28] provides a generalizable basis for scalable MPC solutions without requiring human interference in model calibration. Although higher-order models would perform well in ideal scenarios, our practical experience indicates that implementing second-order approaches, which consider the envelope's thermal capacitance, presents

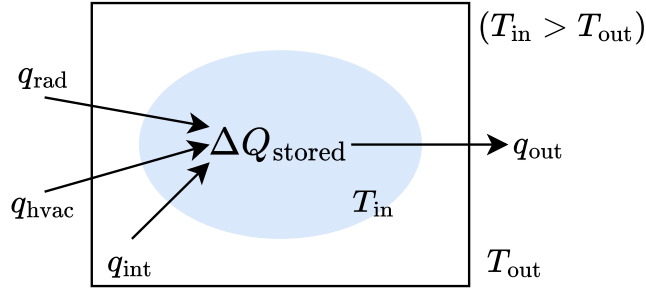


Figure 1: Conservation of thermal energy in a building. Here $\Delta Q_{\text{stored}} = \frac{dQ_{\text{stored}}}{dt}$ describes the rate of change of the thermal energy stored by the indoor air mass over time t .

significant challenges at an industrial scale. These challenges arise primarily due to the introduction of additional latent states and the difficulties in achieving robust parameter estimation from noisy data.

According to the basic physics principle of energy conservation, the change in the thermal energy stored by a system must be equal to the sum of heat flows entering and leaving the system. Applying this and adopting the notation in Figure 1, the thermal energy balance equation for a building can be written as:

$$\frac{dQ_{\text{stored}}}{dt} = q_{\text{hvac}} + q_{\text{out}} + q_{\text{rad}} + q_{\text{int}}, \quad (5)$$

where $\frac{dQ_{\text{stored}}}{dt}$ is the rate of change of thermal energy stored by the indoor air mass with respect to time, q_{hvac} is the heat flow from the heating, ventilation, and air conditioning (HVAC) system, q_{out} is the heat flow through the building envelope, q_{rad} is the heat flow from solar irradiation, and q_{int} is the combined heat flow from various internal heat sources within the building. Here, all right-hand side terms are nonnegative except for q_{out} , assuming that the indoor temperature is greater than the outdoor temperature.

Let us consider that q_{hvac} is brought to the system by a single radiator, which is also a straight pipe, thus assuming the heat flows from other heat sources are negligible. Furthermore, we treat the conductive thermal resistance of the envelope and the convective thermal resistances at its boundary air layers as a single lumped thermal resistor. Expanding the terms in (5) according to heat transfer equations, rearranging them, and denoting the unknown physical coefficients as the parameter vector $\theta \in \mathbb{R}^d$, yields a first-order ordinary differential equation (ODE) for indoor temperature:

$$\frac{dT_{\text{in}}}{dt} = \theta_1(T_{\text{sup}} - T_{\text{in}}) + \theta_2(T_{\text{out}} - T_{\text{in}}) + \theta_3\Phi_{\text{rad}} + \psi(t), \quad (6)$$

where T_{sup} is the space heating supply water temperature, T_{in} is the indoor temperature, T_{out} is the outdoor temperature, and Φ_{rad} is the global horizontal irradiation intensity of the sun. For the q_{int} term in (5), even a simplified physical formula cannot be derived. However, it can be assumed that the effect of this term has some kind of temporal profile, which can be learned from the data. In this work, the hours of the week are divided into 24 business-day and 24 non-business-day hours (weekends and public holidays), summing up to 48 hourly disturbance profiles for internal sources. Thus, q_{int} is written as an indicator function ψ mapping time t to 48 parameters based on the hour of the week. The variables in the other terms are obtained as measured inputs.

Linear state-space models (LSSM) are extensively used in control theory, time series analysis, and dynamical system modeling [29, 30, 27]. Therefore, it is convenient to formulate (6) as an LSSM by including process and observation noise terms, assumed to be Gaussian with zero mean and unknown covariances. This yields the following probabilistic representation for state transition:

$$\begin{aligned} \hat{x}^{(t)} &= (1 - \theta_1 - \theta_2)\hat{x}^{(t-1)} + \begin{bmatrix} \theta_1 & \theta_2 & \theta_3 & 1 \end{bmatrix} \begin{bmatrix} T_{\text{sup}}^{(t)} \\ T_{\text{out}}^{(t)} \\ \Phi_{\text{rad}}^{(t)} \\ \psi(t) \end{bmatrix} + \mathcal{N}(0, \theta_4^{-1}) \\ y^{(t)} &= \hat{x}^{(t)} + \mathcal{N}(0, \theta_5^{-1}), \end{aligned} \quad (7)$$

where $\hat{x}^{(t)}$ is the estimate of the indoor temperature state at time t , and $y^{(t)}$ is the indoor temperature measured at time t . In this work, the time resolution is hourly, and thus $t - j$ denotes the time at j hours prior to t . Collectively, the model parameters, noise parameters, and hourly profile parameters result in the LSSM described in (7) having a total of $D = 53$ parameters. Moreover, let us denote N as the number of total observations, such that $\mathbf{y} \in \mathbb{R}^N$.

The state and parameter estimation for the LSSM model (7) is implemented through the Bayesian framework introduced in 2.1. The joint posterior is expressed as

$$p(\hat{\mathbf{x}}, \boldsymbol{\theta}, \boldsymbol{\alpha} \mid \mathbf{y}) \propto p(\mathbf{y} \mid \hat{\mathbf{x}}, \boldsymbol{\theta})p(\hat{\mathbf{x}} \mid \boldsymbol{\theta})p(\boldsymbol{\theta} \mid \boldsymbol{\alpha})p(\boldsymbol{\alpha}), \quad (8)$$

where $p(\mathbf{y} \mid \hat{\mathbf{x}}, \boldsymbol{\theta})$ is the likelihood function after observing the data \mathbf{y} and $p(\hat{\mathbf{x}} \mid \boldsymbol{\theta})$ is the state prior probability. Both of these are Gaussian densities derived based on (7). Furthermore, we assign conjugate-exponential priors to the remaining terms in (8) (Gaussian and Gamma distributions, respectively) such that

$$p(\boldsymbol{\theta} \mid \boldsymbol{\alpha}) = \prod_{i=1}^D \mathcal{N}(\theta_i \mid 0, \alpha_i^{-1}) \quad p(\boldsymbol{\alpha}) = \prod_{i=1}^D \mathcal{G}(\alpha_i \mid a, b), \quad (9)$$

where the hyperparameters a and b are endowed with non-informative priors (Uniform distributions).

Due to the model's application in large-scale industrial settings, employing sampling-based methods like MCMC for posterior inference is impractical. This is primarily due to the complex geometry of the posterior and the fact that evaluating the posterior for a single sample requires a complete solution of the Kalman filter [27, 31]. Consequently, we seek an approximate solution of the posterior in (8) using variational inference as described in 2.1.1, by assuming the following factorization with respect to the model unknowns:

$$p(\mathbf{Z} \mid \mathbf{y}) \approx q(\mathbf{Z}) = q(\hat{\mathbf{x}})q(\boldsymbol{\theta})q(\boldsymbol{\alpha}), \quad (10)$$

where we denote $\mathbf{Z} = \{\hat{\mathbf{x}}, \boldsymbol{\theta}, \boldsymbol{\alpha}\}$ as a set of all unknowns in (8). Each component of the factorized variational approximation in (10) has the same family as the prior on the respective unknown variable, with its own reference parameters. To find these parameters, the ELBO in (3) is maximized using the posterior (8) and its approximation (10) via the Variational Message Passing (VMP) algorithm [26]. Given our conjugate-exponential assumptions, VMP offers a computationally efficient solution for the posterior approximation, while still offering a full probabilistic framework for state and parameter estimation, unlike methods such as the maximum a posteriori estimator. Both the VMP method for parameter estimation and the Kalman filter updates for the reference LSSM model are implemented using the software package *BayesPy*, introduced in [32].

2.3. Deep learning models

Deep learning (DL), a subset of machine learning, employs artificial neural networks comprising multiple layers to model intricate patterns in data. DL architectures learn hierarchical feature representations by transforming input data through multiple computational layers [33]. Model parameters are optimized through iterative training procedures, typically using large-scale datasets and gradient-based optimization methods.

This work focuses on supervised learning, in which models are trained to make predictions based on labeled input-output pairs: $\{\mathbf{X}, \Delta\mathbf{y}\}$. Our inputs are defined as $\mathbf{X} \in \mathbb{R}^{N \times L \times M}$, where N is the number of samples, L is the sequence length (the number of preceding historical instances considered for the input variables given time t), and M is the number of input variables. Similarly to our reference model, the input variables of the DL models implemented in this work (presented in Table 1) are designed to incorporate physics-based feature engineering. Therefore, instead of having one input dimension for each variable, some of the variables are combined to reflect their physical correlations related to the thermodynamical system: $T_{sup} - T_{in}$ and Φ_{rad} quantify the heat brought to the building by the heating system and solar irradiation, while $T_{out} - T_{in}$ describes the heat that leaks through the building's envelope into the environment. The disturbance effect from internal heat sources is modeled by using a function ξ , which simply maps time t to an integer value based on the hour of the week: 1–24 for non-business-day and 25–48 for business-day hours. Additionally, the azimuth and elevation angles of the sun, α_{azi} and α_{ele} , are included, calculated based on the building's GPS coordinates using the software package *pvlb* [34, 35]. These two additional variables enhance the modeling of the solar effect based on seasonality and building orientation. Finally, because DL models are capable of modeling complex non-linear relationships such as thermal lag effects, each input sequence matrix $\mathbf{X}^{(t)} = [\mathbf{x}^{(t-6)}, \dots, \mathbf{x}^{(t)}] \in \mathbb{R}^{L \times M}$ in \mathbf{X} contains

Variable	Description	Unit
$T_{sup} - T_{in}$	ΔT between supply water and inside air	$^{\circ}\text{C}$
$T_{out} - T_{in}$	ΔT between outside and inside air	$^{\circ}\text{C}$
Φ_{rad}	Global horizontal irradiation of the sun	W / m^2
α_{ele}	Elevation angle of the sun	$^{\circ}$
α_{azi}	Azimuth angle of the sun	$^{\circ}$
$\xi(t)$	An integer value based on the hour of the week	-

Table 1: Input variables of the DL models.

$L = 7$ latest realizations of the $M = 6$ input variables in Table 1. The length of the input sequence $L = 7$ was selected based on experimenting with various values ranging from 1 to 48.

To incorporate the physics of the modeled system given the input variables and their connection to (6), the DL models are trained to predict the change in indoor temperature $\Delta y^{(t)} = T_{in}^{(t+1)} - T_{in}^{(t)}$ instead of indoor temperature directly. Our previous experience indicates that with machine learning models, this approach results in more precise and physically meaningful predictions [9]. Thus, the outputs $\Delta \mathbf{y} \in \mathbb{R}^N$ represent the differences between the indoor temperature measurements of successive hours. As mentioned in 2.2, the time resolution of the observed data used in this work is hourly.

2.3.1. Deterministic deep learning model

Among NN architectures, RNNs are the most commonly used for modeling sequential data. They differ from standard feedforward networks in their ability to incorporate feedback loops, allowing them to utilize previous model states in their computations [36]. However, standard RNNs often face challenges such as vanishing or exploding gradients [37]. To address these issues, LSTMs were developed, incorporating internal gating mechanisms that allow the learning of long-term dependencies in sequential data [38]. LSTMs are specifically designed to mitigate the vanishing gradient problem by employing a technique called adaptive forgetting to reset model memory at appropriate time intervals [39].

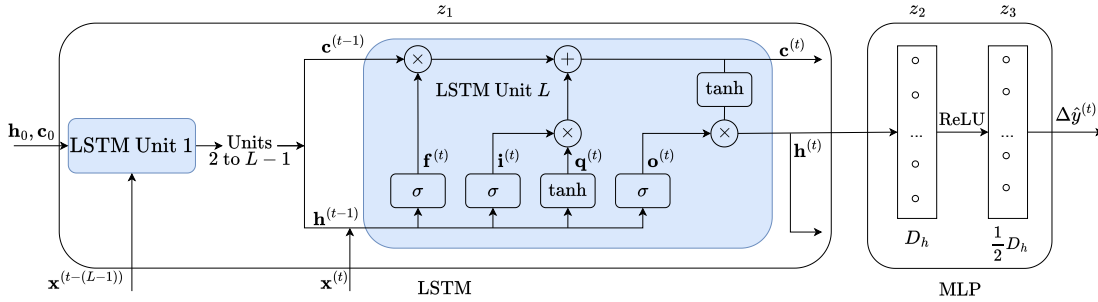


Figure 2: Illustration of an LSTM layer with L LSTM units connected to an MLP with two linear layers. The weights and biases in the LSTM are represented in stacked form as the vector \mathbf{z}_1 . Similarly, the weights and biases of the MLP layers are grouped into \mathbf{z}_2 and \mathbf{z}_3 , respectively.

The structure of an LSTM layer consists of L hidden LSTM units that are connected recursively. Each unit has a forget gate $\mathbf{f}^{(t)}$, an input gate $\mathbf{i}^{(t)}$, and a candidate memory gate $\mathbf{q}^{(t)}$, collectively responsible for managing the model memory, the cell state $\mathbf{c}^{(t)}$, by determining which stored information should be discarded and which new information should be inserted. The output gate $\mathbf{o}^{(t)}$ is needed when combining the information contained in the output (hidden state representation) of the previous LSTM unit $\mathbf{h}^{(t-1)}$, the current input to the unit $\mathbf{x}^{(t)}$, and the updated cell state $\mathbf{c}^{(t)}$. The mathematical formulas for the gate operations are given by [40]:

$$\begin{aligned}
\mathbf{f}^{(t)} &= \sigma(\mathbf{W}_{xf}\mathbf{x}^{(t)} + \mathbf{W}_{hf}\mathbf{h}^{(t-1)} + \mathbf{b}_f) \\
\mathbf{i}^{(t)} &= \sigma(\mathbf{W}_{xi}\mathbf{x}^{(t)} + \mathbf{W}_{hi}\mathbf{h}^{(t-1)} + \mathbf{b}_i) \\
\mathbf{q}^{(t)} &= \tanh(\mathbf{W}_{xg}\mathbf{x}^{(t)} + \mathbf{W}_{hg}\mathbf{h}^{(t-1)}) \\
\mathbf{o}^{(t)} &= \sigma(\mathbf{W}_{xo}\mathbf{x}^{(t)} + \mathbf{W}_{ho}\mathbf{h}^{(t-1)} + \mathbf{b}_o),
\end{aligned} \tag{11}$$

where σ denotes the sigmoid activation function, \mathbf{W}_{xi} , \mathbf{W}_{xf} , \mathbf{W}_{xo} , \mathbf{W}_{hi} , \mathbf{W}_{hf} , \mathbf{W}_{ho} are weight parameters, $\mathbf{x}^{(t)}$ is the input data sequence, and \mathbf{b}_i , \mathbf{b}_f , \mathbf{b}_o are bias parameters. Cell state $\mathbf{c}^{(t)}$ and hidden state $\mathbf{h}^{(t)}$

are then updated by:

$$\begin{aligned} \mathbf{c}^{(t)} &= \mathbf{f}^{(t)} \mathbf{c}^{(t-1)} + \mathbf{i}^{(t)} \mathbf{q}^{(t)} \\ \mathbf{h}^{(t)} &= \mathbf{o}^{(t)} \tanh(\mathbf{c}^{(t)}), \end{aligned} \quad (12)$$

where \mathbf{W}_{xg} and \mathbf{W}_{hg} are weight parameters, and \mathbf{b}_o is a bias parameter.

We construct our deterministic DL model architecture as follows. An LSTM layer encodes the information in an input sequence $\mathbf{X}^{(t)} = [\mathbf{x}^{(t-(L-1))}, \dots, \mathbf{x}^{(t)}] \in \mathbb{R}^{L \times M}$ into hidden states $[\mathbf{h}^{(t-(L-1))}, \dots, \mathbf{h}^{(t)}] \in \mathbb{R}^{L \times D_h}$. The combined information in the final hidden state representation $\mathbf{h}^{(t)}$ is decoded into a scalar prediction $\Delta \hat{y}^{(t)}$ by a multilayer perceptron (MLP) [36]. The MLP block is built from two linear layers connected by the ReLU activation function. The input dimensions of the linear layers are D_h and $\frac{1}{2}D_h$, respectively. Based on previous experiments with different hidden dimensionalities, $D_h = 2^{10}$ was selected [9]. This model architecture, which we refer to as *LSTM+MLP*, is visualized in Figure 2, and mathematically, we can write the forward action of the model given the inputs as

$$\Psi(\mathbf{X}; \mathbf{z}) = (\Psi^{\text{LSTM}}(\mathbf{z}_1) \circ \Psi^{\text{MLP}}(\mathbf{z}_2, \mathbf{z}_3))(\mathbf{X}), \quad (13)$$

where $\Psi^{\text{LSTM}}(\mathbf{z}_1)$ denotes the LSTM, and $\Psi^{\text{MLP}}([\mathbf{z}_2, \mathbf{z}_3])$ denotes the MLP computation. The parameters of the LSTM unit are denoted as \mathbf{z}_1 , the parameters for the first linear layer are denoted as \mathbf{z}_2 and the parameters for the second linear layer used as the output layer are denoted as \mathbf{z}_3 . Thus, all model parameters can be collectively expressed as $\mathbf{z} = [\mathbf{z}_1, \mathbf{z}_2, \mathbf{z}_3]$.

Finally, the loss function used in LSTM+MLP (13) training is the mean absolute error (MAE):

$$\text{MAE} = \frac{1}{N} \sum_t \left| \Delta y^{(t)} - \Delta \hat{y}^{(t)} \right|, \quad (14)$$

where $\Delta \hat{y}^{(t)} = \Psi(\mathbf{X}^{(t)}; \mathbf{z})$ is the prediction scalar computed by the model at a given time instance t .

2.3.2. Partially stochastic deep learning model

Bayesian Neural Networks (BNNs) incorporate probabilistic modeling into conventional neural networks (NNs) by treating the parameters as random variables rather than fixed values. This allows for uncertainty quantification in predictions. The Bayesian aspect arises from assigning prior distributions to the weights and biases, and in this context, the training amounts to estimating the corresponding posterior distribution using Bayes' theorem [41].

Not all parameters in a BNN need to be stochastic to achieve theoretical expressivity and gain in predictive performance [42]. With a smaller optimized parameter space, partially stochastic NNs can outperform fully stochastic NNs in training time. However, careful selection of the stochastic layer is crucial, as not all architectures may meet the criteria for effective probabilistic prediction. The idea is to split the parameter space into two sets, such that the parameter vector can be written as $\mathbf{z} = [\mathbf{z}_D, \mathbf{Z}_R]$. Here, \mathbf{z}_D represents the deterministic parameters for which point estimates are learned, while \mathbf{Z}_R denotes the random parameters for which a distribution, or an approximation of it, is determined. The random parameters \mathbf{Z}_R can be inferred jointly with the deterministic parameters or separately through a two-stage training process [42].

There are several alternatives on how to select the random parameters \mathbf{Z}_R . A common method involves isolating a specific layer and assigning all its parameters to \mathbf{Z}_R . Building upon the LSTM+MLP model (see 2.3.1) and experimenting with different layer parameterizations, we found that choosing the first linear layer as the stochastic layer yielded the best results in terms of predictive performance and computational cost. Thus, we propose a partially stochastic DL model architecture comprising an LSTM layer, a Bayesian linear layer, ReLU activation, and a standard linear layer. We refer to this model architecture as *LSTM+BNN*. Hence, the primary distinction between this model and the deterministic model described in Section 2.3.1 lies in the treatment of the first linear layer, which is now modeled as a Bayesian linear layer. In this case, the parameters \mathbf{z}_2 are represented as a random vector \mathbf{Z}_R . The parameters of the LSTM layer, \mathbf{z}_1 , and the parameters in the second layer of the MLP, \mathbf{z}_3 , are deterministic, so we lump them together as $\mathbf{z}_D = [\mathbf{z}_1, \mathbf{z}_3]$. This generates a partially stochastic model of the form:

$$\Psi(\mathbf{X}; [\mathbf{Z}_R, \mathbf{z}_D]) = (\Psi^{\text{MLP}}([\mathbf{Z}_R, \mathbf{z}_3]) \circ \Psi^{\text{LSTM}}(\mathbf{z}_1))(\mathbf{X}). \quad (15)$$

The training of the model (15) requires the estimation of the posterior distribution of the parameters \mathbf{Z}_R given the data. This task is computationally intensive in high dimensions as we require MCMC

methods to obtain samples from the posterior [41]. To maintain computational scalability, variational inference (see 2.1.1) is commonly performed, finding an approximating density to the posterior by maximizing the ELBO. Following (3), the ELBO for this task is expressed as:

$$\text{ELBO}(q) = \mathbb{E}_q \left[\|\Delta \mathbf{y} - \Psi(\mathbf{X}; [\mathbf{Z}_R, \mathbf{z}_D])\|_1 \right] - w_{\text{KL}} D_{\text{KL}}(q(\mathbf{Z}_R) \parallel p(\mathbf{Z}_R)), \quad (16)$$

where $p(\mathbf{Z}_R)$ is the prior distribution of the random parameters set as Gaussian $\mathcal{N}(\mathbf{0}, \beta^2 \mathbf{I})$. The likelihood term corresponds to a standard multivariate Laplace distribution, which is essentially the probabilistic version of the MAE loss in (14). A weighted KL divergence is employed to address the potential scale difference between the KL divergence term and the likelihood term, with a weight of $w_{\text{KL}} = 10^{-3}$ applied to effectively balance these terms. Note that the likelihood component ensures that the parameters fit the data effectively, while the KL divergence maintains consistency with the prior distribution.

The approximating density q is assumed to be Gaussian $\mathcal{N}(\boldsymbol{\mu}_R, \boldsymbol{\sigma}_R^2 \mathbf{I})$, enabling the KL divergence term in (16) to be efficiently evaluated in closed form. During training, the optimization process iteratively updates $\boldsymbol{\mu}_R, \boldsymbol{\sigma}_R$ (for the random parameters) and \mathbf{z}_D (deterministic parameters) to minimize the negative ELBO. Specifically, at each forward pass through the model and for each sample in \mathbf{X} , the uncertain parameters \mathbf{Z}_R are drawn from the current $\mathcal{N}(\boldsymbol{\mu}_R, \boldsymbol{\sigma}_R^2 \mathbf{I})$, and these values are incorporated into the likelihood component. Meanwhile, the deterministic parameters \mathbf{z}_D are optimized directly during the training loop. This section concludes with a sketch of our approach in Algorithm 1, illustrating the main components of our model and its training process.

Algorithm 1: LSTM+BNN: forward action and training sketch.

$\mathbf{X} \in \mathbb{R}^{N \times L \times M}, \Delta \mathbf{y} \in \mathbb{R}^N$ $\mathbf{h}_0 \in \mathbb{R}^{D_h} \leftarrow \mathbf{0}$ $\mathbf{c}_0 \in \mathbb{R}^{D_h} \leftarrow \mathbf{0}$ $p(\mathbf{Z}_R) \leftarrow \mathcal{N}(\mathbf{0}, \beta^2 \mathbf{I})$ $w_{\text{KL}} \leftarrow 10^{-3}$ Initialize model parameters $\boldsymbol{\mu}_R, \boldsymbol{\sigma}_R, \mathbf{z}_D$ Initialize Minimum validation loss $\leftarrow \infty$ procedure TRAINING(\mathbf{X}) $\mathbf{X} = \{\mathbf{X}_{\text{train}} \in \mathbb{R}^{N_{\text{train}} \times L \times M}, \mathbf{X}_{\text{val}} \in \mathbb{R}^{N_{\text{val}} \times L \times M}\}$ $\Delta \mathbf{y} = \{\Delta \mathbf{y}_{\text{train}} \in \mathbb{R}^{N_{\text{train}}}, \Delta \mathbf{y}_{\text{val}} \in \mathbb{R}^{N_{\text{val}}}\}$ for $i = 1$ to <i>epochs</i> do end Draw $\mathbf{Z}_R \sim q(\mathbf{Z}_R)$ $\Delta \hat{\mathbf{y}}_{\text{train}} \leftarrow \Psi(\mathbf{X}_{\text{train}}; [\mathbf{Z}_R, \mathbf{z}_D])$ Training loss $\leftarrow \text{MAE}(\Delta \hat{\mathbf{y}}_{\text{train}}, \Delta \mathbf{y}_{\text{train}}) + w_{\text{KL}} D_{\text{KL}}(q(\mathbf{Z}_R) \parallel p(\mathbf{Z}_R))$ Back propagate loss to compute gradients w.r.t. $\boldsymbol{\mu}_R, \boldsymbol{\sigma}_R, \mathbf{z}_D$ Update $\boldsymbol{\mu}_R, \boldsymbol{\sigma}_R, \mathbf{z}_D$ based on learning rate and gradients $q(\mathbf{Z}_R) \leftarrow \mathcal{N}(\boldsymbol{\mu}_R, \boldsymbol{\sigma}_R^2 \mathbf{I})$ Draw $\mathbf{Z}_R \sim q(\mathbf{Z}_R)$ $\Delta \hat{\mathbf{y}}_{\text{val}} \leftarrow \Psi(\mathbf{X}_{\text{val}}; [\mathbf{Z}_R, \mathbf{z}_D])$ Validation loss $\leftarrow \text{MAE}(\Delta \hat{\mathbf{y}}_{\text{val}}, \Delta \mathbf{y}_{\text{val}}) + w_{\text{KL}} D_{\text{KL}}(q(\mathbf{Z}_R) \parallel p(\mathbf{Z}_R))$ if <i>Validation loss</i> < <i>Minimum validation loss</i> then end Save LSTM+BNN model with current parameters $\boldsymbol{\mu}_R, \boldsymbol{\sigma}_R, \mathbf{z}_D$ as the Best model Minimum validation loss \leftarrow Validation loss return Best model	<div style="text-align: right;">▷ Training data</div> <div style="text-align: right;">▷ Initial LSTM hidden state</div> <div style="text-align: right;">▷ Initial LSTM cell state</div> <div style="text-align: right;">▷ Prior of BNN parameters</div> <div style="text-align: right;">▷ Define weight for KL divergence</div> <div style="text-align: right;">▷ See equation (15)</div> <div style="text-align: right;">▷ Adam optimizer</div> <div style="text-align: right;">▷ See equation (15)</div>
---	--

3. Experiments

3.1. Dataset

The building-specific datasets were collected by a private company specializing in MPC for centrally-heated residential buildings. For a total of $S = 100$ buildings, the datasets contain hourly time series data between years 2017 and 2022. The indoor temperature data represent the averages of sensor measurements from each apartment in the buildings. The space heating supply water temperature data are measured at

the building-specific heating substations. The outdoor temperature and the solar irradiation data are from the professional weather data provider of the company, fetched for the buildings based on their GPS coordinates.

Since the heating season in northern climates spans September to May, only data from these months are considered. During the summer months, the heating systems are shut off, and therefore the indoor temperature cannot be affected by controlling the supply water temperature of the space heating circuit.

3.2. Model implementations

Given the unique thermodynamics of each building and its heating system, models are trained separately for each of the S buildings. Thus, we end up having S reference models, S LSTM+MLP models, and S LSTM+BNN models. All model formulations can be extended to any building with sufficient data on inputs and outputs, allowing the building-specific thermal dynamics to be expressed through model parameters learned from the data. The DL models are flexible enough to train a single global model for all buildings, enabling the model to transfer information between buildings with similar thermal behavior [9]. While this approach may benefit buildings with insufficient datasets, our aim in this study is to develop building-specific models for cases with comprehensive datasets. In industrial heating MPC applications, one can continuously evaluate different models and the available datasets for different buildings and prediction circumstances, and dynamically choose the model with the best potential for each building and prediction scenario.

Details regarding the inputs and outputs of the reference model are covered in Section 2.2. The state and the parameter estimation of the reference model for each building is performed using the data of the respective building from the last 500 heating season days prior to September 2021.

To train the DL models, all available site-specific data prior to September 2021 are split into *training* and *validation* sets at a 9-to-1 ratio. The models are implemented using software packages `PyTorch` [43] and `torchbnn` [44] as auto-regressive predictors that work on an hourly domain. That is, although the models are used to predict multiple time steps into the future, in the training phase, they are fitted based on their 1-hour forward predictions [9]. Both DL model variants are trained using the Adam optimizer with an initial learning rate of 10^{-4} , decayed by a factor of $\frac{1}{2}$ over 3 scheduled reductions. The number of training epochs are 400 for the LSTM+MLP and 800 for the LSTM+BNN.

3.3. Results

In the MPC application for which the models are developed, control sequences are optimized hourly based on indoor temperature predictions over a prediction horizon of length $H = 48$. Therefore, to maintain the system state at a target value and minimize overheating with MPC, we are particularly interested in the models' short-term predictive performance. However, long-term predictions over the full prediction horizon of length H are crucial for achieving optimal control planning, especially when considering advanced optimization objectives (discussed in Section 1).

The *test* set comprises data from October 2021 to April 2022. Within this date range, $T = 100$ evenly distributed hourly time instances $t \in \mathbb{R}^T$ are selected to comprehensively cover the heating season conditions when testing the models. For each of the S buildings, starting from the selected time instances t , we generate $S \cdot T = 10000$ indoor temperature prediction sequences into a prediction horizon of length $H = 48$ using all three models. Thus, the T_{in} predictions of a single model type are denoted as a matrix $\hat{\mathbf{Y}} \in \mathbb{R}^{(S \cdot T) \times H}$.

The ΔT_{in} predictions of the DL models are transformed into T_{in} predictions by cumulatively adding the predicted differences to the latest indoor temperature measurement the model had available given a starting point $t \in \mathbf{t}$. Since T_{in} is incorporated in two of the DL models' input variables (see Table 1), after the first prediction, the other predictions into the prediction horizon are affected by the previous predictions. In the reference model, the same applies inherently due to the LSSM formulation.

3.3.1. Prior selection for the partially stochastic deep learning model

The LSTM+BNN model is tested with three prior variances β^2 : 10^{-2} , 10^{-3} , and 10^{-4} . Models trained with each prior variance are used to compute $\hat{\mathbf{Y}} \in \mathbb{R}^{(S \cdot T) \times H}$. We then evaluate the models' predictive performance into different horizon lengths $K \in [1, 6, 48]$ by calculating the Root Mean Squared Errors (RMSEs) w.r.t. T_{in} measurements $\mathbf{Y} \in \mathbb{R}^{(S \cdot T) \times H}$ along the horizon lengths K as

$$\epsilon_i^{hor} = \sqrt{\frac{\sum_{j=1}^K (\mathbf{Y}_{i,j} - \hat{\mathbf{Y}}_{i,j})^2}{K}}, \quad i = 1, \dots, S \cdot T. \quad (17)$$

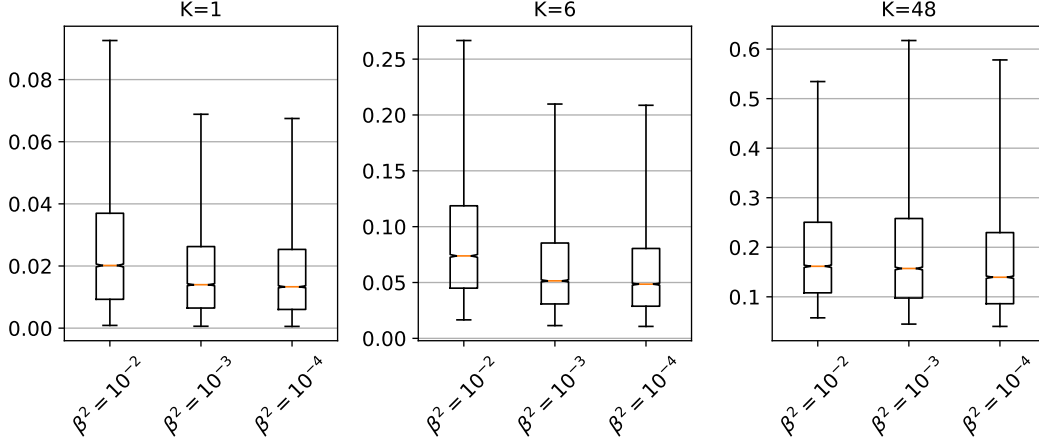


Figure 3: The performance of the LSTM+BNN with different prior variances β^2 as RMSE (17) for different prediction horizon lengths. Orange lines are the RMSE distribution medians, while boxes and whiskers indicate the 50% and 95% confidence intervals, respectively. Note the different scales on the Y-axis.

The respective RMSE distributions are shown in Figure 3.

In addition to predictive performance, the value at which the KL divergence (2) converges during training must be considered. Since KL divergence measures the dissimilarity between the true and the approximate distribution, the closer we get to zero, the better the posterior approximation. Although the LSTM+BNN with a prior variance of 10^{-4} has the best accuracy, its KL divergence for the posterior approximation is 100 times larger than with prior variances of 10^{-2} and 10^{-3} . A small variance in combination with a large KL divergence suggests that the prior is too restrictive. This can lead to instability or overfitting, as the model may not effectively regularize its parameters. Therefore, since the prior $\mathcal{N}(0, 10^{-3}\mathbf{I})$ achieves good predictive performance and low KL divergence for the posterior approximation, it is selected for the LSTM+BNN employed in the comparative experiments of the study.

3.3.2. Predictive performance

For two test samples, Figure 4 shows the predictions of all three models and the predictive uncertainties of the LSTM+BNN model over the 48-hour prediction horizon. Since the uncertainty of the successive LSTM+BNN model predictions are independent, the predictive uncertainties over the prediction horizon are calculated by accumulating the standard deviations of preceding predictions in the sequence.

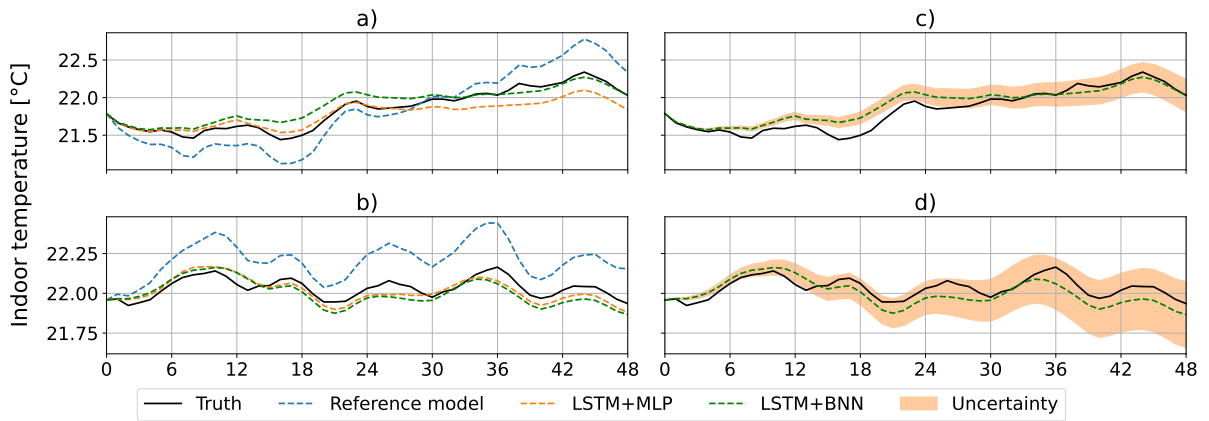


Figure 4: a) and b): 48-hour indoor temperature predictions for two different test samples. c) and d): Predictive uncertainties of the LSTM+BNN for the respective test samples on the left. Uncertainty is quantified as the cumulative standard deviation across each predictions' 10 posterior predictive samples.

To compare the predictive performance of the models across different buildings and heating season conditions, we use the same RMSE metric (17) as we did when selecting the prior variance for the LSTM+BNN in 3.3.1. The results are shown in Figure 5. Both DL models outperform the reference for all three prediction horizon lengths, particularly for longer prediction horizons. The short-term predictions

of the DL models are also significantly more accurate with a tighter RMSE distribution. The predictive performance between the LSTM+MLP and LSTM+BNN models is approximately equal.

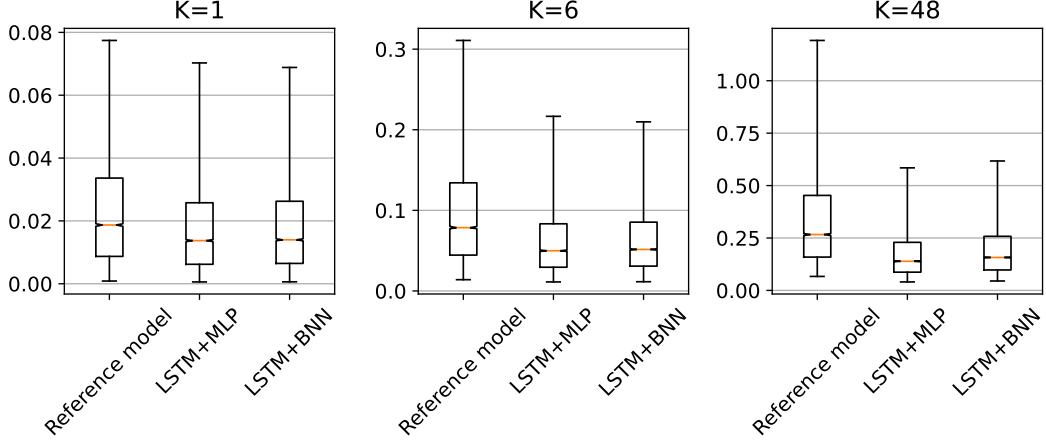


Figure 5: Performance of the three models as RMSE (17) distributions into different prediction horizon lengths. Orange lines are the RMSE distribution medians, while boxes and whiskers indicate the 50% and 95% confidence intervals, respectively. Note the different scales on the Y-axis.

To evaluate how much the predictions $\hat{\mathbf{Y}} \in \mathbb{R}^{(S \cdot T) \times H}$ of each model drift from the measured truth $\mathbf{Y} \in \mathbb{R}^{(S \cdot T) \times H}$ when predicting into the prediction horizon of length $H = 48$, we calculate the average drift over our test samples w.r.t. prediction horizon length using a similar metric to (17), but this time averaging along the test samples:

$$\epsilon_j^{dri} = \sqrt{\frac{\sum_{i=1}^{(S \cdot T)} (\mathbf{Y}_{i,j} - \hat{\mathbf{Y}}_{i,j})^2}{S \cdot T}}, \quad j = 1, \dots, H. \quad (18)$$

The average prediction drifts for all three models are visualized in Figure 6. The results show that the DL models achieve progressively better performance relative to the reference model as the prediction horizon lengthens. Over the test samples, the average performance of the DL models stays similar until the 6-hour horizon length, after which the deterministic LSTM+MLP performs slightly better.

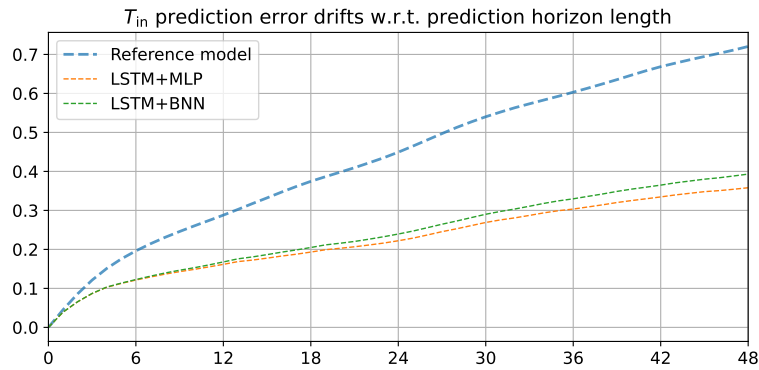


Figure 6: Average prediction drifts across the test samples (18) with the three models.

As discussed earlier, our interest lies more in short-term predictive accuracy than long-term. Hence, to compare the performance of the models using a single metric aligned with what we are interested in, the prediction drift series visualized in Figure 6 is averaged using linear- and sigmoid-shaped weight functions. These functions give decreasing weights for the RMSE values w.r.t. prediction horizon length. The sigmoid function gives more weight to the accuracy of the short-term prediction compared to the linear function (Figure 7). The performance scores calculated this way are shown in Table 2 for all three models.

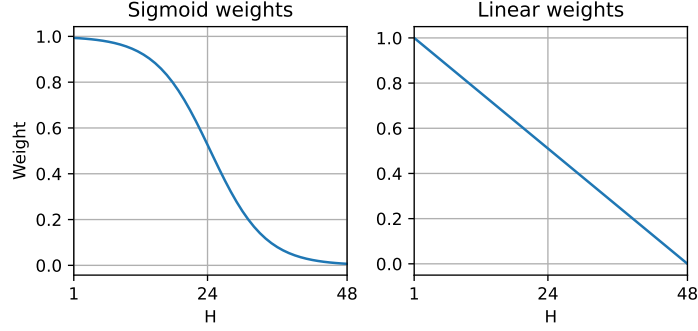


Figure 7: Sigmoid and linear functions used to calculate weighted predictive performance scores in Table 2.

Model	Unweighted	Sigmoid	Linear
Reference	0.436	0.145	0.161
LSTM+MLP	0.225	0.079	0.086
LSTM+BNN	0.247	0.084	0.093

Table 2: Predictive performance scores for the three models calculated by averaging the prediction drifts w.r.t. prediction horizon length (cf. Figure 6) using different weight functions.

3.3.3. Uncertainty quantification

Figure 8 illustrates the average increase in prediction error of the LSTM+BNN with respect to predictive uncertainty. Although the LSTM+BNN performs slightly worse in terms of pure predictive performance compared to its deterministic variant, LSTM+MLP, (see Figure 6 and Table 2), it offers a key advantage in having the ability to quantify the uncertainty present in its predictions. This feature of offering transparency about the potential of the model is highly important when it comes to dynamically selecting the best model for each building and prediction scenario in industrial heating MPC applications.

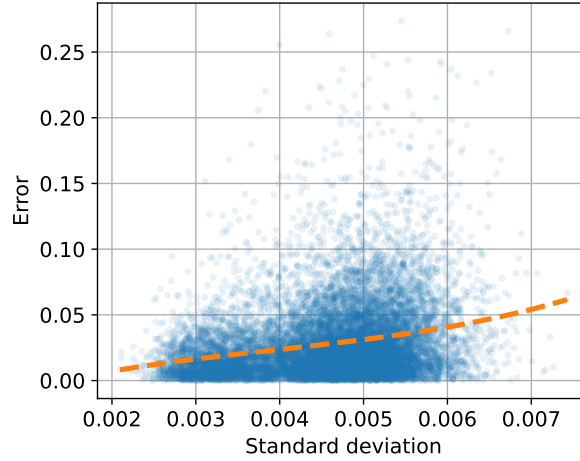


Figure 8: Prediction uncertainties of the LSTM+BNN as standard deviations and the respective prediction errors as MAE for the $S \cdot T$ predictions into a 1-hour prediction horizon. The predictions and the standard deviations for a single test sample are calculated by computing a total of 100 predictions using the building-specific LSTM+BNN models, and taking the mean and the standard deviation, respectively.

3.3.4. Computational costs

The primary drawback of DL models, compared to the reference model, is their computational cost (see Table 3). In the industrial heating MPC application for which the models are developed, control optimization—where models are used for predictions—and model training are separate tasks. For each building, model training is scheduled every other hour, while control optimization is performed hourly.

Given that the reference model is trained using data from the last 500 heating season days, such frequent model updates are not necessary to accurately reflect the recent thermodynamics of a building.

Model	Training time (s)	Prediction time (s)
Reference	5	0.008
LSTM+MLP	180	0.17
LSTM+BNN	360	0.31

Table 3: Computational costs of the models. The training time is the average time taken to train a model for a single building. The prediction time is the average time it took to generate a single 48-hour prediction sequence.

Nonetheless, these updates are currently conducted so often simply due to the minimal computational cost of the reference model’s posterior inference. When integrating the DL models into the MPC framework, it would be adequate to train the model, for instance, only once a week, for buildings with sufficiently comprehensive datasets.

During control optimization, the space heating supply temperature control sequence for the next H hours is initialized based on the most recent optimization results. This sequence is optimized according to various objectives, taking into account recent observations of the system state, current weather forecasts, and model predictions. Due to the effective initialization, the optimization process typically concludes after just a few iterations. Consequently, the longer prediction time of the LSTM+BNN, compared to the reference model, does not impede the implementation of these models in control optimization.

4. Conclusions

We developed a partially stochastic DL architecture, termed LSTM+BNN, for building-specific indoor temperature modeling that incorporates built-in predictive uncertainty quantification.

The method was compared against its deterministic DL variant, LSTM+MLP, and a physics-based Bayesian LSSM used widely in an industrial MPC solution. Experiments were conducted using a large dataset collected from 100 centrally-heated residential buildings, covering different heating season conditions. Both of the DL models outperformed the reference model significantly in both short- and long-term predictions. The 48-hour predictions of the LSTM+BNN models were, on average, 42–43 % more accurate than those of the reference models, depending on the weighting of the short- versus long-term predictions. The improved performance of the DL models comes from their ability to capture complex nonlinear thermodynamics, including thermal lag effects (heat storage in building structures) and solar energy gain variations.

While the two DL variants showed similar accuracy, the partially stochastic version offers transparency by providing a way of quantifying the uncertainty present in its predictions. This feature is highly beneficial for integrating the data-driven model into real-world heating MPC solutions, as model suitability for a building and prediction scenario can be dynamically evaluated prior to each control optimization.

The computational cost of the LSTM+BNN is much higher compared to that of the reference method. However, this does not pose a problem since the models could be trained less frequently when the dataset is comprehensive enough. Therefore, integrating the partially stochastic LSTM+BNN into heating MPC solutions — especially for buildings with comprehensive datasets — has great potential to improve control accuracy, thereby enhancing heating control in terms of energy efficiency, thermal comfort, and more advanced optimization objectives.

Finally, the results of this work motivate and lay the groundwork for further studies on improving indoor temperature modeling related to heating MPC. Hence, we leave as future work the following:

- (i) Understanding carefully which of the learned physical relationships from the data contribute to the enhanced modeling ability of data-driven models, i.e., identifying what is missing from the existing reference model formulation and how it could be improved. For instance, methods like [45] could be used to find interpretable, functional formulations for the input-output mappings learned by the data-driven models.
- (ii) Increasing the inductive bias of the data-driven models by incorporating domain knowledge into the training process, i.e., finding the balance between theory- and data-driven modeling [46, 47, 48, 49]. This could enhance the generalization ability, especially with limited or noisy training data.
- (iii) Heating dynamics of buildings exhibit seasonal patterns, slow trends, and sudden shifts (e.g., from physical modifications). Future work could also focus on adaptive methods that balance learning from new data and discarding outdated information, possibly via time-evolving parameters [50].

- (iv) Further optimization of the partially stochastic LSTM+BNN architecture (e.g., dimension reduction via sensitivity analysis or principal component analysis), and training settings via hyperparameter tuning (batch size, learning rates, initialization) to lower the computational costs.

5. Acknowledgments

We would like to give special thanks to Jaakko Luttinen for his work on the reference method and to Alexander Ilin for his involvement in the conceptualization of the project. Furthermore, we thank Danfoss Leanheat for providing the data used in the study.

This work was supported by the Finnish Ministry of Education and Culture’s Pilot for Doctoral Programmes (Pilot project Mathematics of Sensing, Imaging and Modelling) and Research Council of Finland (Flagship of Advanced Mathematics for Sensing and Imaging and Modeling grant 359183, Centre of Excellence of Inverse Modelling and Imaging grant 353095). The research of Jana de Wiljes has been partially funded by the Deutsche Forschungsgemeinschaft (DFG)- Project-ID 318763901 - SFB1294. Furthermore, this project has received funding from the European Union under the Horizon Europe Research & Innovation Programme (Grant Agreement no. No 101188131 UrbanAIR). Views and opinions expressed are however those of author(s) only and do not necessarily reflect those of the European Union. Neither the European Union nor the granting authority can be held responsible for them.

References

- [1] International Energy Agency (IEA), *World Energy Outlook 2024*, 2024.
- [2] United Nations Environment Programme, *Global Status Report for Buildings and Construction*, 2024.
- [3] M. González-Torres, L. Pérez-Lombard, J. F. Coronel, I. R. Maestre, D. Yan, A review on buildings energy information: Trends, end-uses, fuels and drivers, *Energy Reports* 8 (2022) 626–637.
- [4] D. Ürgüç, L. F. Cabeza, S. Serrano, C. Barreneche, K. Petrichenko, Heating and cooling energy trends and drivers in buildings, *Renewable and Sustainable Energy Reviews* 41 (2015) 85–98.
- [5] R. Fazeli, B. Davidsdottir, J. H. Hallgrímsson, Residential energy demand for space heating in the Nordic countries: Accounting for interfuel substitution, *Renewable and Sustainable Energy Reviews* 57 (2016) 1210–1226.
- [6] Y. Yao, D. K. Shekhar, State of the art review on model predictive control (MPC) in heating ventilation and air-conditioning (HVAC) field, *Building and Environment* 200 (2021) 107952.
- [7] S. Taheri, P. Hosseini, A. Razban, Model predictive control of heating, ventilation, and air conditioning (HVAC) systems: A state-of-the-art review, *Journal of Building Engineering* 60 (2022) 105067.
- [8] J. Drgoňa, J. Arroyo, I. Cupeiro Figueroa, D. Blum, K. Arendt, D. Kim, E. P. Ollé, J. Oravec, M. Wetter, D. L. Vrabie, L. Helsen, All you need to know about model predictive control for buildings, *Annual Reviews in Control* 50 (2020) 190–232.
- [9] A. Häkkinen, Machine learning models for predicting indoor temperature of central-heated residential buildings, Master’s thesis, Aalto University, 2022. Available at: <https://aaltodoc.aalto.fi/items/3cf8831b-d86e-4508-8eca-e8e85577b3d0>.
- [10] L. Ramadan, I. Shahrour, H. Mroueh, F. H. Chehade, Use of machine learning methods for indoor temperature forecasting, *Future internet* 13 (2021) 242.
- [11] C. Xu, H. Chen, J. Wang, Y. Guo, Y. Yuan, Improving prediction performance for indoor temperature in public buildings based on a novel deep learning method, *Building and environment* 148 (2019) 128–135.
- [12] F. Mtibaa, K.-K. Nguyen, M. Azam, A. Papachristou, J.-S. Venne, M. Cheriet, LSTM-based indoor air temperature prediction framework for HVAC systems in smart buildings, *Neural Computing and Applications* 32 (2020) 17569–17585.
- [13] L. Ma, Y. Huang, J. Zhang, T. Zhao, A model predictive control for heat supply at building thermal inlet based on data-driven model, *Buildings (Basel)* 12 (2022) 1879.
- [14] F. Elmaz, R. Eyckerman, W. Casteels, S. Latré, P. Hellinckx, CNN-LSTM architecture for predictive indoor temperature modeling, *Building and environment* 206 (2021) 108327.
- [15] B. Jiang, H. Gong, H. Qin, M. Zhu, Attention-LSTM architecture combined with Bayesian hyperparameter optimization for indoor temperature prediction, *Building and environment* 224 (2022) 109536.
- [16] Z. Fang, N. Crimier, L. Scanu, A. Midelet, A. Alyafi, B. Delinchant, Multi-zone indoor temperature prediction with LSTM-based sequence to sequence model, *Energy and buildings* 245 (2021) 111053.
- [17] F. Bünnig, B. Huber, A. Schalbeter, A. Aboudonia, M. Hudoba de Badyn, P. Heer, R. S. Smith, J. Lygeros, Physics-informed linear regression is competitive with two machine learning methods in residential building MPC, *Applied Energy* 310 (2022) 118491.
- [18] D. T. Mirikitani, N. Nikolaev, Recursive bayesian recurrent neural networks for time-series modeling, *IEEE Transactions on Neural Networks* 21 (2010) 262–274.
- [19] R. Wen, K. Torkkola, B. Narayanaswamy, D. Madeka, A multi-horizon quantile recurrent forecaster, *arXiv preprint arXiv:1711.11053* (2017).
- [20] A. M. Alaa, M. van der Schaar, Frequentist uncertainty in recurrent neural networks via blockwise influence functions, in: H. Daumé III, A. Singh (Eds.), *Proceedings of the 37th International Conference on Machine Learning*, volume 119, PMLR, 2020, pp. 175–190. doi:[10.48550/arXiv.2006.13707](https://doi.org/10.48550/arXiv.2006.13707).
- [21] C. Xu, Y. Xie, Conformal prediction interval for dynamic time-series, in: M. Meila, T. Zhang (Eds.), *Proceedings of the 38th International Conference on Machine Learning*, volume 139, PMLR, 2021, pp. 11559–11569.
- [22] K. Stankevičiūtė, A. M. Alaa, M. van der Schaar, Conformal time-series forecasting, in: *Advances in Neural Information Processing Systems*, volume 34, 2021, pp. 14485–14497.

- [23] A. Gelman, J. Carlin, H. Stern, D. Dunson, A. Vehtari, D. Rubin, Bayesian Data Analysis, Third Edition, Chapman & Hall/CRC Texts in Statistical Science, Taylor & Francis, 2013.
- [24] M. I. Jordan, Z. Ghahramani, T. S. Jaakkola, L. K. Saul, An Introduction to Variational Methods for Graphical Models, Springer Netherlands, Dordrecht, 1998, pp. 105–161. doi:[10.1007/978-94-011-5014-9](https://doi.org/10.1007/978-94-011-5014-9).
- [25] C. Bishop, Pattern recognition and machine learning, Information science and statistics, Springer, 2006.
- [26] J. Winn, C. M. Bishop, Variational message passing, Journal of Machine Learning Research 6 (2005) 661–694.
- [27] J. Luttinen, Fast variational Bayesian linear state-space model, in: Machine Learning and Knowledge Discovery in Databases, Springer, 2013, pp. 305–320.
- [28] A. Ionesi, On modeling and estimation techniques towards on-line applications in building energy management systems, 2019.
- [29] R. H. Shumway, D. S. Stoffer, Time series analysis and its applications, Springer, 2000.
- [30] D. E. Kirk, Optimal control theory - An introduction, 1 Edition., Dover Publications, 1998.
- [31] S. Särkkä, L. Svensson, Bayesian Filtering and Smoothing, 2 Edition., Cambridge University Press, 2023.
- [32] J. Luttinen, Bayespy: Variational bayesian inference in python, Journal of Machine Learning Research 17 (2016) 1–6.
- [33] Y. LeCun, Y. Bengio, G. Hinton, Deep learning, Nature (London) 521 (2015) 436–444.
- [34] W. F. Holmgren, C. W. Hansen, M. A. Mikofski, pvlib python: a python package for modeling solar energy systems, Journal of Open Source Software 3 (2018) 884.
- [35] K. S. Anderson, C. W. Hansen, W. F. Holmgren, A. R. Jensen, M. A. Mikofski, A. Driesse, pvlib python: 2023 project update, Journal of Open Source Software 8 (2023) 5994.
- [36] I. Goodfellow, Y. Bengio, A. Courville, Deep learning, MIT Press, 2016.
- [37] H. Hewamalage, C. Bergmeir, K. Bandara, Recurrent neural networks for time series forecasting: Current status and future directions, International journal of forecasting 37 (2021) 388–427.
- [38] S. Hochreiter, J. Schmidhuber, Long short-term memory, Neural computation 9 (1997) 1735–1780.
- [39] F. A. Gers, J. Schmidhuber, F. Cummins, Learning to forget: Continual prediction with LSTM, Neural Computation 12 (2000) 2451–2471.
- [40] D. Mora-Mariano, A. Flores-Tlacuahuac, Bayesian LSTM framework for the surrogate modeling of process engineering systems, Computers & Chemical Engineering 181 (2024) 108553.
- [41] R. M. Neal, Bayesian learning for neural networks, volume 118, Springer Science & Business Media, 2012.
- [42] M. Sharma, S. Farquhar, E. Nalisnick, T. Rainforth, Do bayesian neural networks need to be fully stochastic?, in: Proceedings of The 26th International Conference on Artificial Intelligence and Statistics, volume 206 of *Proceedings of Machine Learning Research*, PMLR, 2023, pp. 7694–7722.
- [43] A. Paszke, S. Gross, F. Massa, A. Lerer, J. Bradbury, G. Chanan, T. Killeen, Z. Lin, N. Gimelshein, L. Antiga, A. Desmaison, A. Kopf, E. Yang, Z. DeVito, M. Raison, A. Tejani, S. Chilamkurthy, B. Steiner, L. Fang, J. Bai, S. Chintala, Pytorch: An imperative style, high-performance deep learning library, in: Advances in Neural Information Processing Systems 32, Curran Associates, Inc., 2019, pp. 8024–8035.
- [44] S. Lee, H. Kim, J. Lee, Graddiv: Adversarial robustness of randomized neural networks via gradient diversity regularization, IEEE Transactions on Pattern Analysis and Machine Intelligence (2022).
- [45] M. Cranmer, Interpretable machine learning for science with pysr and symbolicregression.jl, 2023. [arXiv:2305.01582](https://arxiv.org/abs/2305.01582).
- [46] M. Raissi, P. Perdikaris, G. Karniadakis, Physics-informed neural networks: A deep learning framework for solving forward and inverse problems involving nonlinear partial differential equations, Journal of Computational Physics 378 (2019) 686–707.
- [47] J.-H. Bastek, W. Sun, D. M. Kochmann, Physics-informed diffusion models, 2025. [arXiv:2403.14404](https://arxiv.org/abs/2403.14404).
- [48] R. T. Q. Chen, Y. Rubanova, J. Bettencourt, D. Duvenaud, Neural ordinary differential equations, 2019. [arXiv:1806.07366](https://arxiv.org/abs/1806.07366).
- [49] C. Rackauckas, Y. Ma, J. Martensen, C. Warner, K. Zubov, R. Supekar, D. Skinner, A. Ramadhan, A. Edelman, Universal differential equations for scientific machine learning, 2021. [arXiv:2001.04385](https://arxiv.org/abs/2001.04385).
- [50] L. Rimella, N. Whiteley, Hidden markov neural networks, Entropy 27 (2025).